The IRM
Quarterly
Winter 2022-23, Vol. 32 No. 4
ISSN: 2152-1972

Inside...

Practical Magnetism X: A review of the low temperature AC susceptibility frequency-dependence of multidomain (titano)magnetite.

Dario Bilardello
Institute for Rock Magnetism
dario@umn.edu

A lot has been written about the frequency-dependence of susceptibility (χ) of superparamagnetic (SP) nanoparticles and their (un)blocking peaks below room temperature, to the point that low-temperature peaks of both in-phase (χ') and out-of-phase (χ") susceptibility are most-commonly only described in terms of particles within the SP to single domain (SD) continuum (e.g. Till et al., 2011; Volk et al., 2018).

However, less has been written about the low-temperature susceptibility behavior of multi domain (MD) grains, which consistently exhibit low temperature frequency-dependent peaks and/or "anomalies" in both χ' and χ". This behavior was first observed by Iwauchi (1976) (Fig. 1), and, as already proposed by Iida et al. (1968), the Fe_3O_4 relaxation below 50 K had been interpreted as the electron transfer between four crystallographically equivalent iron ions ($2Fe^{2+}$ and $2Fe^{3+}$) on the octahedral sites in the Verwey ordering of electrons. The origin of the behavior has been confirmed since, although the mechanism through which it manifests is somewhat less poorly understood. In any case, it is useful to provide a short review of the topic to familiarize researchers with the existing observations, understanding, and pertinent references.

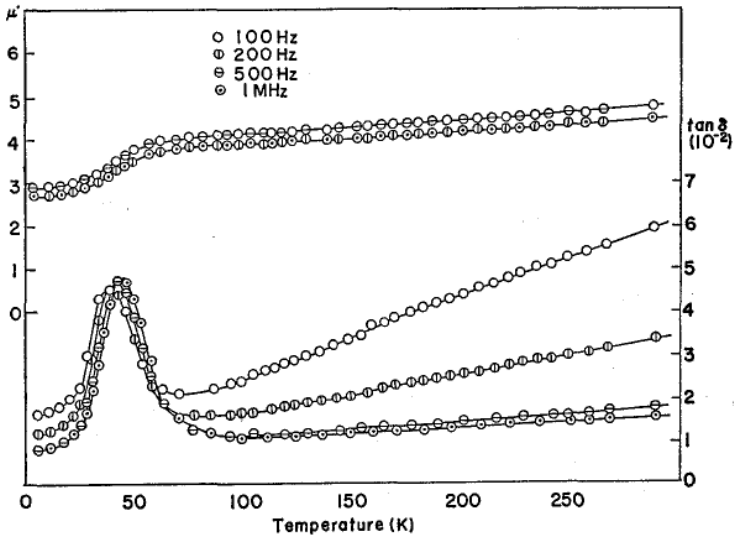

Figure 1: First observation of frequency dependence of "magnetic permeability" μ' for a 19 mm synthetic Fe_3O_4 sample at ~40 K between 4.2 and 300 K by Iwauchi et al. (1976): $\mu' = L'/L_0$, where L' is the real part of the inductance L_0, and the magnetic loss tangent (tan δ)= L''/L', where L" is the imaginary part of L_0. Note that the frequencies used were 100-500 kHz (not 100-500 Hz, as reported in the figure) and 1 MHz, as stated in the body of the article and reported in subsequent figures.

Magnetic Susceptibility Essential Review

Magnetic susceptibility, k or $\chi = M / H$, where k typically denotes dimensionless volume-normalized susceptibility, often reported in "SI" units, or μSI (= 10-6 SI) and χ is mass-normalized, in units of m^3/kg, is most commonly measured in fields of ~200-300 A/m or less, although AC field intensities used in different instruments may range from 2 A/m up to 700 A/m. The small fields typically applied in general do not cause irreversible magnetizations, making low-field susceptibility a widely applied non-destructive technique to characterize the magnetic response of different geological materials.

The three classes of magnetic materials are diamagnetic, paramagnetic and ferromagnetic (comprising both ferrimagnetic and antiferromagnetic), and immersed in an external field, a rock's constituent minerals will contribute positively or negatively to the bulk magnetic susceptibility. Ferromagnetic iron oxides have larger susceptibilities than the diamagnetic and paramagnetic minerals that make up the matrix and, when present in sufficient concentrations, will dominate the susceptibility response. Consequently, magnetic susceptibility is a strongly concentration-dependent bulk property.

Unlike in a constant (DC) field, measuring in an oscillating (AF or AC) field $H_0 e^{i\omega t}$, where the field varies with time as $H = H_0 \cos(\omega t)$, may cause the magnetic response to lag behind the field peaks, so that $M = M_0 \cos(\omega t - \delta)$, where δ is the phase lag and ω is the angular frequency. M can be decomposed into in-phase ("real") and 90° out-of-phase ("imaginary" or "quadrature") components: $M = M' \cos(\omega t) + M'' \sin(\omega t)$, where $\tan(\delta) = M''/M'$ and $(M_0)^2 = M'^2 + M''^2$. Accordingly, AC susceptibility χ is a

cont'd. on pg. 11...

Visiting Fellow Reports

Assessing the use of thermal fluctuation tomography on resolving the SP/SD grain size distribution in London Underground air pollution particulate samples

Hassan Sheikh
Cambridge University

has57@cam.ac.uk

Air pollution in indoor settings is not very well characterised. The London Underground is one such microenvironment that has high levels of particulate matter (PM) air pollution concentrations, marked by the abundance (50% of total PM) of iron oxide nanoparticles (Smith et al., 2020). We used a combination of magnetic and microscopy methods to characterise the iron oxide particles (Sheikh et al., 2022). Bulk room temperature magnetic measurements and first order reversal curves (FORCs) indicated the presence of superparamagnetic (SP), single domain (SD) and pseudo single domain (PSD) magnetic particles. Scanning electron microscopy (SEM) and transmission electron microscopy (TEM) observations showed particles had nanoscale dimensions in the range of 5-500 nm; many of which were agglomerated to form large clusters and only a few were isolated particles. The microscopy observations supported bulk experimental magnetic results and using low temperature magnetic data, we were also able to quantify the superparamagnetic (SP) size fraction of particles. These are the finest particles (<20 nm) in a particulate matter (PM2.5) size fraction.

A primary aim for my visiting fellowship was to compare our experimental data with modelled approaches to reaffirm the presence of sub-micron sized particles. Using Field-Cooled (FC) and Zero-Field Cooled (ZFC) remanence experiments performed on a Magnetic Properties Measurement System (MPMS-3), we had already established the absence of Verwey transition in low temperature measurements, hinting at the absence of magnetite and a signature of maghemite (Fig. 1). I also wanted to assess the amount of superparamagnetic fraction (SP) in our samples using Low temperature (LT) SIRM measurements. To quantify the SP contribution, we estimated ΔM, compared to the total IRM (at 2.5 T and 10 K), for the selected sample. This is the difference in remanence between RT-SIRM (10 K) and ZFC curve (at 10 K). An approach I wanted to test during the fellowship was the application of thermal fluctuation tomography (TFT) technique (Jackson et al., 2006) on air pollution PM filters, which has been attempted here for the first time. The idea was to use TFT modelling to determine and compare the statistical grain size distribution of the

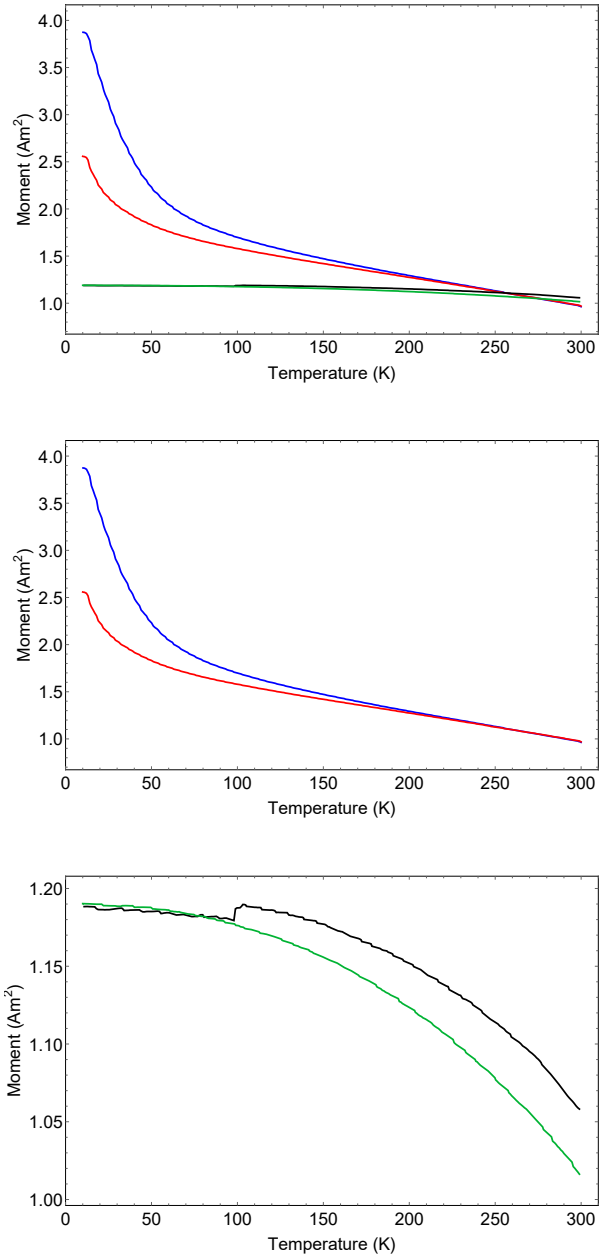

Figure 1: Low-temperature remanent magnetization curves for 180487-92. Top: Zero-field cooled (red), and field cooled (blue) (ZFC and FC) curves do not show any evidence for Verwey transition or dampened transition (usually seen for surface oxidized magnetite). Bottom: RT-SIRM warming (black) and cooling curves (green) do not show any evidence of Verwey transition at 120-125 K or lower temperatures.

very fine magnetic particles below the PM2.5 (particles with diameter less than 2.5 micron) size threshold. This is to distinguish larger, clustered particles which appear to be physically larger in diameter but consist of several individual grains of magnetic particles.

The SP fraction in our sample was estimated to be around 67% (i.e., particles less than 20 nm in diameter) using the LT-SIRM data from Fig. 1, making it ideal to apply TFT modelling. TFT measurements were performed using a Lake Shore vibrating sample magnetometer (VSM) equipped with a Single Stage Variable Temperature (SSVT) option. We measured backfield remanent magnetisation curves from 0 to 300 mT with a 10 mT field step between a temperature range of 100 K- 300

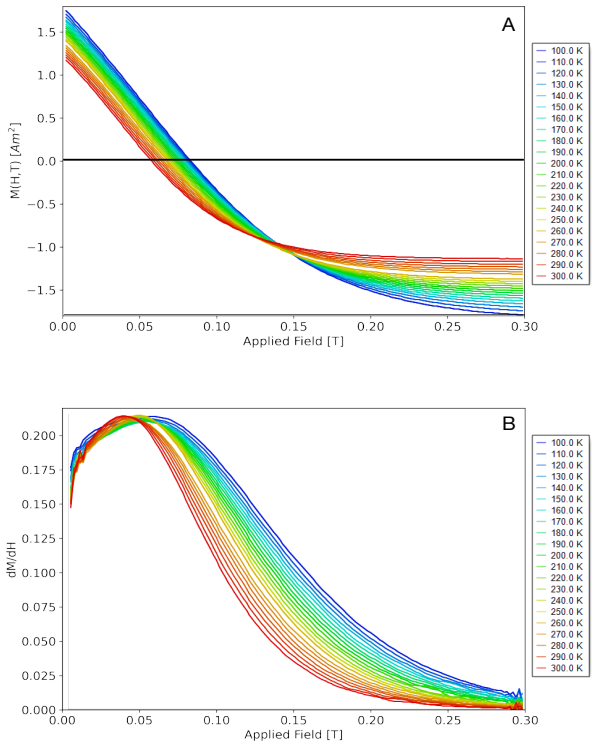

Figure 2: (a) shows remanent magnetisation as a function of applied DC backfield (b) dM/dH vs applied DC backfield. Temperature ranges from 100- 300 K at 10 K increments, field from 0-300 mT at 5 mT field steps.

K at 10 K intervals (Fig. 1)

The backfield curves (Fig. 2) were then processed to quantify the distribution f(V, H_k) of particle volume (V) and micro coercivity (H_k) of the ultrafine particles in the sample. TFT (Jackson et al., 2006) follows Dunlop's (Dunlop, 1965) methodology of determining joint distribution for different particle V and anisotropies by using temperature-dependent switching field distributions to reconstruct f(V, H_k) for ensembles that contain SP and SD particles.

We used values of maghemite for the model parameters i.e., saturation magnetisation M_s 400 kA/m (at room temperature) and Curie temperature (T_c) at 920 K. The size and shape distribution of magnetic particles calculated from TFT for sample 180487-92 gives a mode at aerodynamic diameter or length (L) = 114 nm and width/length aspect ratio (W/L) = 0.57.

Low temperature saturation isothermal remanent magnetisation (LT-SIRM) warming, and cooling curves do not show presence of a Verwey transition, I interpret this as the abundance of maghemite.

Direct current (DC) backfield remanence curves have a total of 1200 datapoints (60 field steps at each of the 20 temperatures from 100-300 K). These measurements involved saturating the samples with a forward-field and subsequently applying and removing incremental backfields and measuring the magnetic remanence at each specific temperature, which magnetises all the grains f(V, H_k) which are stable at that temperature. Further application and removal of increasingly negative DC fields, reverses the moments of grains with distribution f(V, H_k) below a blocking contour. The reconstructed

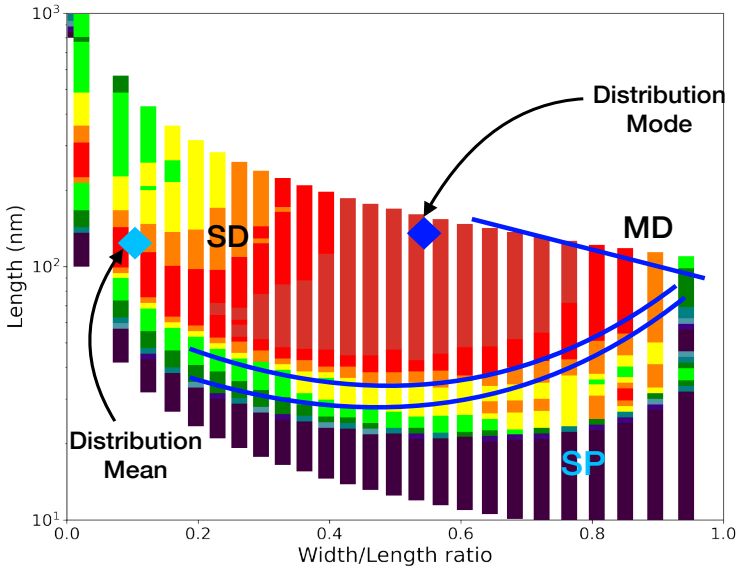

Figure 3: Plot of modelled particle length against width/length (1.0 is a cube). Distribution of grains calculated using back field remanence curves, distribution mode and mean are marked on the figure where the mode is more representative of the sample.

grain distribution model (900 iterations) for our sample shows a wide range of f(V, H_k) distribution, with a mode (V, $\mu_0 H_{k0}$) = (4.0 × 10−23 m^3, and 222 mT) and (w,w/L) = (144.9, and 0.574). The mode particle diameter is slightly higher than from observations made under the TEM but is more consistent with 3D tomography grain-size data (Sheikh et al., 2022) where the W/L aspect ratio lies closer to the observed aspect ratio. Generally, a wide grain size and shape distribution is observed (red region), with the head and tail extending over SP-SD grain sizes and aspect ratio of 0.20-0.90 (Fig. 2). This magnetic grain size distribution is consistent with our microscopy data which showed SP/SD particles agglomerated to form larger clusters (Sheikh et al. 2022). There is a spread of particle size distribution in our example (Fig. 2), which (Jackson et al., 2006) has attributed to be along the dominant blocking contour orientation.

I note that the magnetic results from TFT modelling are in broad agreement with experimental data from bulk magnetic measurements. However, the Butler-Banerjee plot (Fig. 3) does not show any meaningful data below the 12 nm length. I believe our results might have been more consistent with the microscopy data if the TFT measurements were done at lower temperatures of 10 K to map the entire spectrum of the superparamagnetic fraction. A more detailed description of the usage of TFT technique in air pollution samples will be discussed in a separate publication. The fellowship to IRM allowed me to explore the feasibility of the TFT technique on air pollution samples, which has not been done before.

Acknowledgements

I would like to thank Dr Maxwell Brown for his immense help in performing the experiments and fruitful discussions about the data, without which this would have not been possible. I would also like to thank my supervisor, Prof Richard J Harrison, who encouraged me to apply for the fellowship and explained fundamental concepts

of TFT technique.

References

Dunlop, D. J. (1965). Grain Distributions in Rocks Containing Single Domain Grains. Journal of Geomagnetism and Geoelectricity, 17(3–4), 459–471. https://doi.org/10.5636/jgg.17.459

Jackson, M., Carter-Stiglitz, B., Egli, R., & Solheid, P. (2006). Characterizing the superparamagnetic grain distribution f (V , H k) by thermal fluctuation tomography: THERMAL FLUCTUATION TOMOGRAPHY. Journal of Geophysical Research: Solid Earth, 111(B12), n/a-n/a. https://doi.org/10.1029/2006JB004514

Louis, N. (1949). Théorie du traînage magnétique des ferromagnétiques en grains fins avec application aux terres cuites. 5, pp.99-136.

Sheikh, H. A., Tung, P. Y., Ringe, E., & Harrison, R. J. (2022). Magnetic and microscopic investigation of airborne iron oxide nanoparticles in the London Underground. Scientific Reports, 12(1), 20298. https://doi.org/10.1038/s41598-022-24679-4

Smith, J. D., Barratt, B. M., Fuller, G. W., Kelly, F. J., Loxham, M., Nicolosi, E., Priestman, M., Tremper, A. H., & Green, D. C. (2020). PM2.5 on the London Underground. Environment International, 134, 105188. https://doi.org/10.1016/j.envint.2019.105188

The Hunt for Hemozoin- 2.0

Mallory Cox
Yale University

Mallory.cox@yale.edu

The scientific community lacks consensus regarding the presence of the malaria parasite (*Plasmodium spp.*) in human populations of the ancient Americas before European colonization. Since the early 20th century, the most widely accepted paradigm posited that *Plasmodium vivax* (*P. vivax*) was imported to the New World in the late 15th century with European colonizers and that *Plasmodium falciparum* (*P. falciparum*) was introduced in the 16th -19th centuries with the Transatlantic slave trade. Current evidence for *Plasmodium spp.* in the ancient Americas is limited to two studies. One study conducted by Gertszen et al. (2012) presented strong evidence for the presence of *P. vivax* in mummies from Peru and Chile (1000 BC-1400 AD), with the discovery of *P. vivax* antigens in 40% of the livers and spleens analyzed in the study (N=155). The other study was my MA thesis, the Hunt for Hemozoin (Cox, 2018), which identified preliminary evidence for the heme molecular ion and hemozoin crystal (malaria biomarkers) in a female individual from Puerto Rico (900 AD) using mass spectrometry and electron microscopy. That individual is part of the collection of human remains I am analyzing for my dissertation to investigate the presence of malaria in populations of the ancient Americas by identifying *Plasmodium spp.* ancient DNA and Plasmodium-derived hemozoin in skeletal remains from archaeological contexts. My dissertation study collection includes 105 long bone samples from 49 individuals representing 15 archaeological sites, eight in Panama (2800 BC- 1550 AD) and seven in Puerto Rico (400 BC-1200 AD). The individuals (n= 30) from the Panamanian collection (Smithsonian Tropical Research Institute) represent multiple biogeographical contexts and are ideally suited to address the primary goals of this research; detailed reports on the collections include observations of skeletal lesions associated with malaria (Smith-Guzman 2015), but further analyses are required to confirm the etiology of the lesions.

By tradition, paleopathology has focused on the identification and study of diseases based on the analysis of pathological lesions in human skeletal remains. In the case of acute infections, this approach has limitations because an individual may die quickly without time for lesions to develop (Wood et al. 1992). Because of this "osteological paradox," paleopathologists must extend their methodologies beyond those traditionally employed; the emergent field of paleomicrobiology is well-suited to fill this niche. In addition to amplifying ancient pathogenic DNA, paleomicrobiology can detect pathogen-specific antigens (diagnostic), parasite eggs and bodies, and other disease biomarkers. Hemozoin (referred to as Hz hereafter), an iron-bearing crystalline pigment that sequesters in bone marrow cavities of malaria-infected individuals, is a robust biomarker for malaria identification in living populations. Because of the highly alkaline pH required to break down the Hz, we expect this material to remain in long bones' highly protected marrow cavities for extended periods of time, depending on the soil conditions and microenvironment (Setzer, 2014).

The magnetic properties of the Hz biomarker are exploited in clinical settings of malaria research to allow researchers to separate the infected cells from the uninfected for downstream analyses (Roch et al., 2019). Reports demonstrate that the magnetic susceptibility of the infected red blood cell increases linearly as the parasite matures (Hackett, 2009). In recent years, nuclear magnetic resonance magnetometry has been used to identify malaria-infected individuals with submicroscopic parasitemia at orders of magnitude lower than several other diagnostic methods (Fook Kong et al., 2015). The literature contains conflicting reports on the bulk magnetic properties of Hz at room temperature. While some researchers report Hz crystals as exhibiting only superparamagnetic (SP) behavior, other groups argue for observing paramagnetism in synthetic and natural Hz (Inyushin et al., 2016, Roch et al., 2019). One way to resolve this seeming conflict would be to test the idea that both behaviors exist in an unfiltered Hz sample. In fact, our hypotheses support this alternative conclusion. The first steps included measuring synthetic Hz and the heme monomers (essentially the building blocks of Hz crystals) to test our preliminary hypotheses, which can be summarized as follows:

-A single heme monomer is sub-nanometer in size. Therefore, we predict that the heme monomer, if at all (ferro)magnetic, would exhibit superparamagnetic behavior at room temperature based on size alone or other-

wise would exclusively exhibit paramagnetism.

-The average Plasmodium-derived Hz crystal is around 200 x 300 x 1000 nm; therefore, we predicted that the synthetic Hz crystal would exhibit either superparamagnetic or even weak ferromagnetic behavior at room temperature.

-Finally, a natural Hz sample obtained in a clinical laboratory that hasn't been filtered would likely contain variable concentrations of Hz crystals, dimers (a dimer is composed of 2 heme monomers), and the heme monomer, leading to the observations of mixed magnetic behaviors of superparamagnetism and paramagnetism.

To test our hypotheses, we measured the heme monomer (hemin-Sigma Aldrich), and synthetic hemozoin (synthetic Hz-InVivogen) in detail at room temperature. First, we utilized the Vibrating Sample Magnetometer (VSM) to collect hysteresis loops to identify the bulk magnetic properties of each material. One significant observation was that the heme monomer appeared to be superparamagnetic, displaying no hysteresis and an approach to saturation > 500 mT (Fig 1), which was in line with our hypotheses. However, a First Order Reversal Curve (FORC) for the heme monomer revealed a distinct ferromagnetic component that is more obvious than from the hysteresis loops (Fig 2), which was to our surprise. We plan to follow this up with scanning electron microscopy and repeated analyses. We hypothesize that the ferromagnetic behavior we observed in the heme monomer may result from "evolved aggregates" of heme, meaning that they are not fully crystalline yet. We further confirmed that synthetic Hz exhibits dominant paramagnetic behavior at room temperature with weak underlying ferromagnetism. We also performed several low-temperature experiments on the MPMS3, and we are still in the process of reviewing those data. At the same time, we have conducted a whole gamut of magnetic experiments on natural hemozoin crystals extracted from infected individuals. These will be compared to the results from the synthetic materials in an attempt to draw first-time correlations. We expect to publish our full results within the year.

These are important, groundbreaking observations that would otherwise not have been possible if it weren't for the support provided by my 2022 Research Fellowship to the Institute for Rock Magnetism and the assistance of staff scientists in-house. With the data collected during the fellowship at the IRM, specifically the high level of detail permitted by the magnetometry experiments at high fields and variable temperatures, our understanding of the magnetic properties of hemozoin has greatly enhanced. These data improve our understanding of the magnetic properties of hemozoin, bringing us one step closer to identifying malaria in the archaeological record of the pre-colonial Americas.

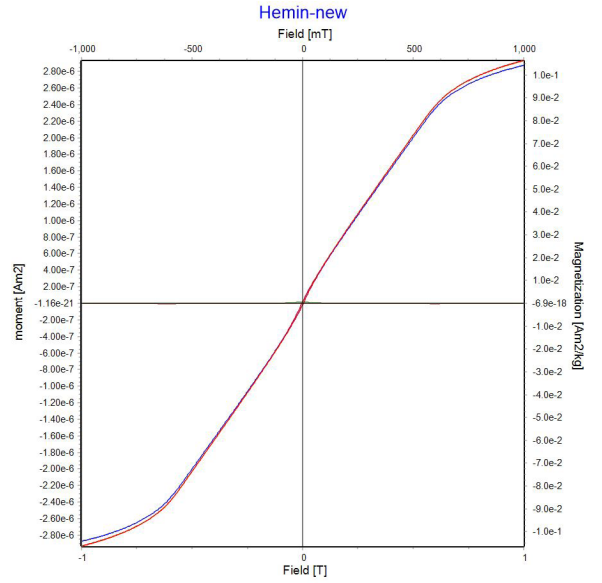

Figure 1: Hysteresis Loop - Heme Monomer

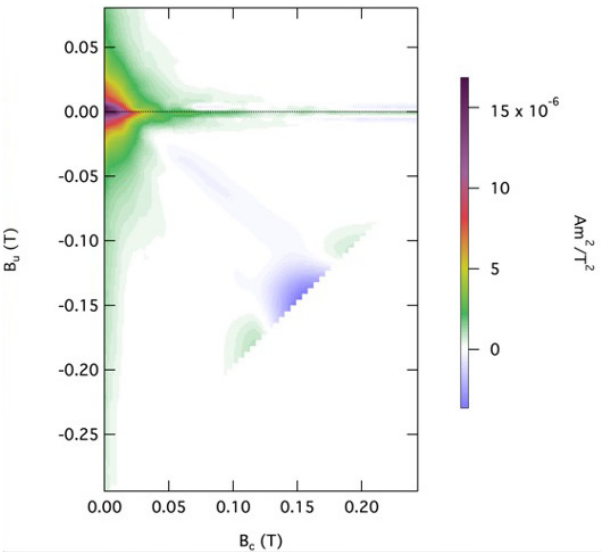

Figure 2: Figure 2. FORC - Heme Monomer

References

Cox, M. D. "Malaria in the prehistoric Caribbean: the hunt for hemozoin." (2018).

Fook Kong, T., Ye, W., Peng, W., Hou, H., Preiser, P. R., Nguyen, N., and J. Han. "Enhancing malaria diagnosis through microfluidic cell enrichment and magnetic resonance relaxometry detection." Scientific reports 5, no. 1 (2015): 11425

Gerszten, E., Marvin J. A., and B. Maguire. "Paleopathology in South American mummies: a review and new findings." Pathobiology 79, no. 5 (2012): 247-256.

Hackett, S., Hamzah, J., Davis, T. M. E., and T. G. St Pierre. "Magnetic susceptibility of iron in malaria-infected red blood cells." Biochimica et Biophysica Acta (BBA)-Molecular Basis of Disease 1792, no. 2 (2009): 93-99

Inyushin, M., Kucheryavih, Y., Kucheryavih, L., Rojas, L., Igor Khmelinskii, I., and V. Makarov. "Superparamagnetic properties of hemozoin." Scientific reports 6, no. 1 (2016): 1-9

Roch, A. Prodéo, J., Pierart, C., Muller, R. N., and P. Duez. "The paramagnetic properties of malaria pigment, hemozoin, yield clues to a low-cost system for its trapping and determination." Talanta 197 (2019): 553-557

Setzer, T. J. "Malaria detection in the field of paleopathology: A meta-analysis of the state of the art." Acta tropica 140 (2014): 97-104

Smith-Guzmán, N. E. "The skeletal manifestation of malaria: An epidemiological approach using documented skeletal collections." American Journal of Physical Anthropology 158, no. 4 (2015): 624-635

Recent and Current Visiting Fellows

Period 2022b

Andrew Ichimura
Chemistry & Biochemistry, San Francisco State University: *Magnetic Properties of Lunar Soils and Lunar Soil Simulants.*

Brendan Reilly
Scripps Institution of Oceanography, UC San Diego: *Towards an understanding of the depths of authigenic ferrimagnetic iron sulfide formation using Scotia Sea drill cores.*

Elias Mansbach
Earth, Atmospheric, and Planetary Science, MIT: *Exploring Martian Crustal Magnetization Through Laboratory Alteration Experiments*

Katie Bristol
Department of Geological Sciences, University of Florida: *Investigating the Spatial Distribution of High-Coercivity Magnetizations within Clinkers using Quantum Diamond Microscopy.*

Mallory Cox
Department of Anthropology, Yale University: *The Malaria project.*

Michael Corolla
Department of Anthropology, Yale University: *Archaeomagnetic Dating of Middle Senegal Valley Furnaces.*

Michael Volk
Earth Sciences, Utrecht University: *Probing changes to the magnetic carriers due to small magnitude earthquake slip.*

Rosa de Boer
Earth Sciences, Utrecht University: *The first geological application of micromagnetic tomography.*

Theodore Bobik
Earth, Environment, and Planetary Science, Brown University: *New insights to the First Americans and trends of arctic tundra fire through the exceptionally long (> 200kyr) sediment record from Seward, Alaska.*

Period 2023a

Bruno Daniel Leite Mendes
Structural Geology and Tectonics, Karlsruhe Institute of Technology: *Interaction between chemical alteration and magnetic domain size changes during temperature dependent magnetic susceptibility measurements.*

Claudio Robustelli Test
Dipartimento di Scienze della Terra, Università degli Studi di Torino: *Magnetic fingerprint of hydrothermal alteration across the South Atlantic subseafloor.*

Hannah Robutka
School of Earth and Ocean Sciences, University of Victoria: *Tracking the evolution of Fe mineralogy in mid-ocean ridge hydrothermal plumes using magnetics.*

Hong Yang
Department of Geophysics, Stanford University: *Using field- dependent magnetic susceptibility to quickly characterize magnetic mineralogy for submarine basalts.*

James Hepworth
School of Geography, Earth and Environmental Sciences, University of Plymouth: *Novel insights into paleomagnetism of serpentinized peridotites from the Oman and Troodos ophiolites.*

Joonas Wasiljeff
Environmental Solutions, Geological Survey of Finland:
FERMAID - Ferromanganese Concretion- Archives of Ecosystem Variability, Climate Forcing and Anthropogenic Impact on the Baltic Sea.

Melissa Sikes
Department of Geosciences, University of Wisconsin-Milwaukee: *Investigation of paleomagnetic behavior of the Snake River Plain lava flows, southeastern Idaho.*

Ron Shaar
The Institute of Earth Sciences, The Hebrew University of Jerusalem: *Magnetic properties of marine sediments and speleothems.*

IMPORTANT ANNOUNCEMENT!

Visiting Fellow reports are an integral aspect of the IRM Quarterly and are of tremendous value to us, as they demonstrate that the IRM's mission is being fulfilled. For all Visiting Fellows who visited since (and including) August 2022, it was made a requirement to submit a VF Report. Failure to do so will be factored into the evaluation for successive fellowships. Provided the higher volume of reports, these will not be as thoroughly edited and commented on as is currently done.

Current Articles

A list of current research articles dealing with various topics in the physics and chemistry of magnetism is a regular feature of the IRM Quarterly. Articles published in familiar geology and geophysics journals are included; special emphasis is given to current articles from physics, chemistry, and materials-science journals. Most are taken from ISI Web of Knowledge, after which they are subjected to Procrustean culling for this newsletter. An extensive reference list of articles (primarily about rock magnetism, the physics and chemistry of magnetism, and some paleomagnetism) is continually updated at the IRM. This list, with more than 10,000 references, is available free of charge. Your contributions both to the list and to the Current Articles section of the IRM Quarterly are always welcome.

Archeomag

Deldicque, D., J. P. Pozzi, C. Perrenoud, C. Falgueres, G. Mahieuxd, A. S. Lartigot-Campin, and J. N. Rouzaud (2022), Traces of fire in a 560,000-year-old occupation soil at Caune de l'Arago: response to the article by Professor Henry de Lumley, Comptes Rendus Geoscience, 354, 47-50, doi:10.5802/crgeos.114.

Lumley, H. D. (2022), Did the first inhabitants of the Caune de l'Arago between 700,000 and 400,000 years BP have domesticated fire? Did they know how to light the fire at will?, Comptes Rendus Geoscience, 354, 41-45, doi:10.5802/crgeos.113.

Tema, E., Y. Santos, R. Trindade, G. A. Hartmann, T. Hatakeyama, F. Terra-Nova, N. Matsumoto, J. Mitsumoto, and M. Gulmini (2023), Archaeointensity record of weak field recurrence in Japan: new data from Late Yayoi and Kofun ceramic artefacts, Geophysical Journal International, 233(2), 950-963, doi:10.1093/gji/ggac498.

Wang, Q. Z., et al. (2022a), New archaeomagnetic directions from Late Neolithic sites in Shandong province, China, Geophysical Journal International, 232(2), 1159-1172, doi:10.1093/gji/ggac381.

Environmental Magnetism

Ayoubi, S., and S. Bahmani (2023), Variation of heavy metals, magnetic susceptibility, and some chemical properties in the Lichen-rock interface on various parent rocks in west of Iran, Physics and Chemistry of the Earth, 129, doi:10.1016/j.pce.2022.103303.

Menendez-Iglesias, D., Rodriguez-Rivas, J. and H. Cabadas-Baez (2022), Late Pleistocene paleoenvironment at a Middle Stone Age archaeological site in Equatorial Guinea: a paleopedological approach, Boletin De La Sociedad Geologica Mexicana, 74(3), doi:10.18268/BSGM2022v-74n3a200622.

Bucko, M. S., T. Magiera, B. Gorka-Kostrubiec, and M. Wawer (2023), Ecological quality of the "Torfowisko pod Weglincem" nature reserve (SW Poland) based on magnetic and geochemical studies, Journal of Applied Geophysics, 208, doi:10.1016/j.jappgeo.2022.104874.

Dong, L. S., et al. (2022), A Eurasian Basin sedimentary record of glacial impact on the central Arctic Ocean during MIS 1-4, Global and Planetary Change, 219, doi:10.1016/j.gloplacha.2022.103993.

Ghosh, R., et al. (2023), Last 10 millennial history of Indian summer monsoon in the Bengal region - a multi-proxy reconstruction from a lacustrine archive, Palaeogeography Palaeoclimatology Palaeoecology, 609, doi:10.1016/j.palaeo.2022.111308.

Jiang, H., Q. Yin, A. Berger, L. Wei, Z. Wu, X. Wei, and W. Shi (2023), Orbitally and galactic cosmic forced abrupt climate events during the last glacial period, Quaternary Science Reviews, 301, doi:10.1016/j.quascirev.2022.107921.

Jordanova, D., B. Georgieva, N. Jordanova, Y. Guyodo, and F. Lagroix (2022), Holocene palaeoenvironmental conditions in NE Bulgaria uncovered by mineral magnetic and paleomagnetic records of an alluvial soil, Quaternary International, 631, 47-58, doi:10.1016/j.quaint.2022.06.009.

Joshi, P., B. Phartiyal, M. Joshi, S. Agrawal, P. Kumar, and R. Sharma (2023), Reconstruction of landscape and climate of the largest drainage basin in the Ladakh Range, NW Trans Himalaya during the last 7000 years, Catena, 223, doi:10.1016/j.catena.2022.106907.

Kadlec, J., I. Svetlik, M. Rybnicek, T. Kolar, F. Stehlik, E. Petrovsky, and H. Grison (2022), Palaeoenvironmental changes and anthropogenic impact recorded in floodplain sediments: A case study from the lower Morava River Basin (Czech Republic), Palaeogeography Palaeoclimatology Palaeoecology, 597, doi:10.1016/j.palaeo.2022.111000.

Li, S., H. Y. Liu, H. Y. Wang, S. W. Feng, X. Y. Yang, Y. K. Zheng, C. Y. Zhu, W. J. Zhao, and Z. Y. Zhang (2023), A rare record of the early and middle Holocene dust export history of the Mongolian Plateau obtained from a crater lake on its southern boundary, Catena, 222, doi:10.1016/j.catena.2022.106847.

Li, Y., S. M. Peng, L. Hao, X. R. Zhou, and H. Y. Li (2022), Interactions of the Westerlies and Asian Summer Monsoon Since the Last Deglaciation in the Northeastern Qinghai-Tibet Plateau, Paleoceanography and Paleoclimatology, 37(11), doi:10.1029/2022pa004548.

Li, Z. Y., M. Sheng, X. S. Wang, K. Jiang, P. Sun, S. Y. Yi, and Z. Y. Yang (2022), Irreversible intensification of the East Asian winter monsoon and aridity in Asian interior linked to the uplifted Tibetan Plateau: Evidence from magnetoclimatology of the Xining loess since 1.3 Ma, Quaternary Science Reviews, 298, doi:10.1016/j.quascirev.2022.107875.

Liu, X. B., J. Chen, W. Yue, Q. Wang, C. Zhan, L. Zeng, J. Song, L. S. Wang, and B. L. Cui (2022), Tracing the source-sink process of fluvio-clastic materials: Magnetic records of surface sediments in the Yangtze River basin, Frontiers in Marine Science, 9, doi:10.3389/fmars.2022.1002335.

Meng, X. Q., G. K. Li, L. W. Liu, X. Y. Long, W. C. Zhao, J. Da, and J. F. Ji (2022), Decoupled paleosol-based proxies in Chinese loess deposits: Role of leaching and illuviation processes, Quaternary Science Reviews, 298, doi:10.1016/j.quascirev.2022.107847.

Mir, J. A., R. A. Dar, M. Vinnepand, C. Laag, C. Rolf, and C. Zeeden (2022), Environmental reconstruction potentials of Loess-Paleosol-Sequences in Kashmir through high-resolution proxy data, Palaeogeography Palaeoclimatology Palaeoecology, 601, doi:10.1016/j.palaeo.2022.111100.

Nims, C., and J. E. Johnson (2022), Exploring the secondary mineral products generated by microbial iron respiration in Archean ocean simulations, Geobiology, 20(6), 743-763, doi:10.1111/gbi.12523.

Qiao, Q. Q., J. D. A. Piper, and Z. Z. Lv (2022), Multivariate Analysis of Magnetic Parameters and Trace Metals in Atmospheric Dustfall and Its Environmental Implications in Northern China, Minerals, 12(12), doi:10.3390/min12121598.

Strbak, O., P. Hnilicova, J. Gombos, A. Lokajova, and P. Kopcansky (2022), Magnetotactic Bacteria: From Evolution to Biomineralization and Biomedical Applications, Minerals, 12(11), doi:10.3390/min12111403.

Wagner, C. L., P. Stassen, E. Thomas, P. C. Lippert, and I.

Lascu (2022), Magnetofossils and Benthic Foraminifera Record Changes in Food Supply and Deoxygenation of the Coastal Marine Seafloor During the Paleocene-Eocene Thermal Maximum, Paleoceanography and Paleoclimatology, 37(10), doi:10.1029/2022pa004502.

Wang, X. X., J. S. Nie, T. Stevens, H. B. Zhang, and W. J. Xiao (2022b), Resolving conflicting models of late Miocene East Asian summer monsoon intensity recorded in Red Clay deposits on the Chinese Loess Plateau, Earth-Science Reviews, 234, doi:10.1016/j.earscirev.2022.104200.

Yang, J. H., D. S. Xia, Z. X. Chen, S. Y. Wang, F. Y. Gao, X. Liu, S. Zhao, L. Zhao, and Y. Liu (2023), Differentiating detrital and pedogenic contributions to the magnetic properties of aeolian deposits in the southern Tibetan Plateau: Implications for paleoclimatic reconstruction, Catena, 220, doi:10.1016/j.catena.2022.106736.

Yang, T., M. J. Dekkers, X. X. Zhao, K. E. Petronotis, and Y. M. Chou (2022), Greigite Formation Modulated by Turbidites and Bioturbation in Deep-Sea Sediments Offshore Sumatra, Journal of Geophysical Research-Solid Earth, 127(11), doi:10.1029/2022jb024734.

Yang, X. Q., S. Wu, S. T. Shang, and Y. Chen (2023), Hydrodynamic variations and human activities have influenced sediment fluxes in the pearl river delta since the late holocene, Frontiers in Earth Science, 10, doi:10.3389/feart.2022.1015697.

Zhang, T., et al. (2022), Orbital forcing of tropical climate dynamics in the Early Cambrian, Global and Planetary Change, 219, doi:10.1016/j.gloplacha.2022.103985.

Zhao, X. Q., W. G. Zhang, F. Wang, Q. L. Vu, and Y. Saito (2023), Late Holocene sediment provenance change in the Red River Delta: A magnetic study, Catena, 220, doi:10.1016/j.catena.2022.106685.

Zhong, Y., et al. (2022), Humidification of Central Asia and equatorward shifts of westerly winds since the late Pliocene, Communications Earth & Environment, 3(1), doi:10.1038/s43247-022-00604-5.

Zhu, Y., et al. (2022), Sedimentary records and chronology of the late Pleistocene overbank flooding in the Yellow River source area, NE Tibetan Plateau, Frontiers in Earth Science, 10, doi:10.3389/feart.2022.1021106.

Extraterrestrial and Planetary Magnetism

Fan, Y., et al. (2022), Shidian meteorite, a new fall analog of near-Earth asteroid (101955) Bennu, Meteoritics & Planetary Science, 57(12), 2192-2215, doi:10.1111/maps.13925.

Gurgurewicz, J., D. Mege, F. Schmidt, S. Doute, and B. Langlais (2022), Megashears and hydrothermalism at the Martian crustal dichotomy in Valles Marineris, Communications Earth & Environment, 3(1), doi:10.1038/s43247-022-00612-5.

Mansbach, E. N., J. Shah, W. Williams, C. Maurel, J. F. J. Bryson, and B. P. Weiss (2022), Size Ranges of Magnetic Domain States in Tetrataenite, Geochemistry Geophysics Geosystems, 23(11), doi:10.1029/2022gc010631.

Ruggiu, L. K., et al. (2022), Detection of incipient aqueous alteration in carbonaceous chondrites, Geochimica Et Cosmochimica Acta, 336, 308-331, doi:10.1016/j.gca.2022.09.020.

Sato, M., et al. (2022), Rock Magnetic Characterization of Returned Samples From Asteroid (162173) Ryugu: Implications for Paleomagnetic Interpretation and Paleointensity Estimation, Journal of Geophysical Research-Planets, 127(11), doi:10.1029/2022je007405.

Fundamental and Applied Rock Magnetism

Afremov, L. L., and I. G. Iliushin (2022), Evaluation of the Metastability in Nanodispersed Heterophase Titanomagnetites, Izvestiya-Physics of the Solid Earth, 58(6), 969-980, doi:10.1134/s1069351322060155.

Gribov, S. K., V. P. Shcherbakov, V. A. Tselmovich, and N. A. Aphinogenova (2022), Properties of Thermochemical Remanent Magnetization on Basalt Samples Containing Titanomagnetites with Increased Thermal Stability, Izvestiya-Physics of the Solid Earth, 58(6), 842-858, doi:10.1134/s1069351322060039.

Leao-Santos, M., R. Moraes, Y. G. Li, M. I. Raposo, and B. X. Zuo (2022), Hydrothermal Alteration Zones' Magnetic Susceptibility Footprints and 3D Model of Iron Oxide-Copper-Gold (IOCG) Mineralization, Carajas Mineral Province, Brazil, Minerals, 12(12), doi:10.3390/min12121581.

Liu, D. L., et al. (2022), Magnetic evidence of seismic fluid processes along the East Yibug Chaka Fault, Tibet, Tectonophysics, 838, doi:10.1016/j.tecto.2022.229500.

McCollom, T. M., F. Klein, B. Moskowitz, and P. Solheid (2022), Experimental serpentinization of iron-rich olivine (hortonolite): Implications for hydrogen generation and secondary mineralization on Mars and icy moons, Geochimica Et Cosmochimica Acta, 335, 98-110, doi:10.1016/j.gca.2022.08.025.

Geomagnetism, Paleointensity and Records of the Geomagnetic Field

Bono, R. K., G. A. Paterson, and A. J. Biggin (2022), MCADAM: A Continuous Paleomagnetic Dipole Moment Model for at Least 3.7 Billion Years, Geophysical Research Letters, 49(21), doi:10.1029/2022gl100898.

Goguitchaichvili, A., B. Gomez, M. C. Rathert, V. Lebedev, M. Cervantes, G. Vashakidze, J. Sologashvili, and J. Morales (2022), Further evidence of unstable reverse polarity geomagnetic field across the Olduvai subchron: paleomagnetic and multispecimen paleointensity study on Khertvisi lava flows (Lesser Caucasus), Physics of the Earth and Planetary Interiors, 333, doi:10.1016/j.pepi.2022.106952.

Lloyd, S. J., A. J. Biggin, G. A. Paterson, and P. J. A. McCausland (2022), Extremely weak early Cambrian dipole moment similar to Ediacaran: Evidence for long-term trends in geomagnetic field behaviour?, Earth and Planetary Science Letters, 595, doi:10.1016/j.epsl.2022.117757.

Lund, S. (2022), A summary of paleomagnetic secular variation and excursions for the last 380 ky of the Brunhes normal polarity Chron, Physics of the Earth and Planetary Interiors, 333, doi:10.1016/j.pepi.2022.106923.

Rathert, M. C., A. Carrancho, J. Morales, N. Perez-Rodriguez, V. A. Lebedev, A. Caccavari, N. Vegas, and A. Goguitchaichvili (2022), Multimethod palaeointensity results from a rapidly emitted upper Miocene lava flow sequence in Sao Vicente (Cape Verde): new data for the African record, Geophysical Journal International, 231(1), 215-229, doi:10.1093/gji/ggac173.

Shcherbakova, V. V., V. Y. Vodovozov, G. V. Zhidkov, N. A. Aphinogenova, N. V. Sal'naya, and G. L. Leichenkov (2022), Ultra-Low Geomagnetic Field Intensity in the Mesoproterozoic Based on the Dike Complex Rocks of the Bunger Oasis (1133 Ma, East Antarctica), Izvestiya-Physics of the Solid Earth, 58(6), 859-881, doi:10.1134/s106935132206012x.

Valero, L., A. Garcia-Alix, G. Jimenez-Moreno, J. Camuera, A. Lopez-Aviles, M. J. Ramos-Roman, F. J. Jimenez-Espejo, E. Beamud, E. Maestre, and R. S. Anderson (2023), Evidences of the Blake and Iceland Basin magnetic excursions

in southeastern Iberia and chronological implications for the Padul sedimentary record, Quaternary Geochronology, 74, doi:10.1016/j.quageo.2022.101421.

Magnetic Fabrics and Anisotropy

Banjan M., Crouzet C., Sabatier P., Jomard H., Bajard M., Demory F., Develle A-L., Jenny J.-P., Fanget B., Malet E., Alain P., Julien D., Bichet V., Clapot S., Messager E. (2022): Did the Younger Dryas to Holocene climate transition favour high seismicity rates in the north-western Alps? Sedimentology, https://doi.org/10.1111/sed.13050.

Bubik, M., T. Elbra, J. Francu, S. Kdyr, P. Schnabl, and L. Svabenicka (2022), Post-Cretaceous-Paleogene slumping in the Subsilesian Unit of the Outer Western Carpathians: Biostratigraphic, sedimentary and magnetic records from the Byst?ice section, Geologica Carpathica, 73(6), 561-577, doi:10.31577/GeolCarp.73.6.4.

Chakraborty, R., M. A. Mamtani, S. Tripathi, A. Singh, S. Rakesh, K. Chakrabarti, and D. K. Sinha (2022), Variation in Anisotropy of Magnetic Susceptibility with Depth in the Upper 1 km of the Earth's Crust in Singhbhum Region (India) - First Results, Journal of the Geological Society of India, 98(12), 1665-1670, doi:10.1007/s12594-022-2235-3.

Chen, Q. L., et al. (2022), Thrust Structure and Bidirectional Paleocurrent in the Jingzhushan Formation during the Late Cretaceous in the Nyima Basin, Tibet Plateau, China: Approach of Magnetic Fabric and Zircon Chronology, Minerals, 12(10), doi:10.3390/min12101225.

Cruz, C., H. Sant'Ovaia, W. McCarthy, and F. Noronha (2022), Anisotropy of Out-of-Phase Magnetic Susceptibility: A Non-Standard Approach for Magnetic Subfabrics Determination in Variscan Granites of Iberian Massif, Minerals, 12(11), doi:10.3390/min12111376.

Hu, C. L., C. C. Han, J. H. Ma, L. Deng, and L. F. Zhao (2022), Paleowind Directions over the Tarim Block during the Mesoproterozoic, Northwestern China, Minerals, 12(11), doi:10.3390/min12111435.

Jia, S. F., B. C. Huang, H. L. Lu, Q. Zhao, Y. G. Yan, Y. L. Liang, and Z. Y. Yi (2023), Reconnaissance on the constraint of rock magnetic fabrics on the reliability of remanent magnetization: A case study for Mesozoic detrital rocks from the Indochian Block and red beds from the Shexing Formation of the Linzhou Basin, Lhasa, Chinese Journal of Geophysics-Chinese Edition, 66(1), 301-313, doi:10.6038/cjg2022P0990.

Staneczek, D., R. Szaniawski, and J. Szczygiel (2022), Transpression-driven deformations of the Cho?ske vrchy Mountains (Western Carpathians): Insights from magnetic fabric, Geologica Carpathica, 73(5), 451-471, doi:10.31577/GeolCarp.73.5.4.

Viegas, G., L. Montefalco, E. Yokoyama, C. J. Archanjo, M. I. B. Raposo, K. Seoane, and G. D. Leite (2022), Magnetic fabric of the early-Ediacaran Itapetim monzogranitic pluton: magma flow during oblique extension along strike-slip shear zones (Eastern Brazil), Journal of Structural Geology, 164, doi:10.1016/j.jsg.2022.104738.

Yakupoğlu N., Henry P., Uçarkuş G., Eriş K., Demory F., Crouzet C. and Çağatay N. (2022): Factors Affecting Deposition of Turbidite-Homogenite Units in Kumburgaz Basin, Sea of Marmara: Critical Assessment of Their Use in Submarine Paleoseismology. Marine geology, 452, 10.1016/j.margeo.2022.106900.

Magnetic Mineralogy and Petrology, Other

Ding, T., A. A. Dias, J. Wang, T. T. Tan, J. Liang, B. Wu, and C. H. Tao (2023), Serpentinization and its implications for ultramafic-hosted sulfide mineralization: A case study at the Tianzuo hydrothermal field, 63.5 degrees E Southwest Indian Ridge, Marine Geology, 455, doi:10.1016/j.margeo.2022.106969.

Kettler, R. M., Y. S. He, S. Ke, F. Z. Teng, and D. B. Loope (2022), Iron isotope evidence for siderite precursors to iron oxide concretions from the Navajo Sandstone, Utah (USA), Chemical Geology, 612, doi:10.1016/j.chemgeo.2022.121146.

Li, X. X., A. X. Sheng, Y. F. Ding, and J. Liu (2022), A model towards understanding stabilities and crystallization pathways of iron (oxyhydr)oxides in redox-dynamic environments, Geochimica Et Cosmochimica Acta, 336, 92-103, doi:10.1016/j.gca.2022.09.002.

Sandler, A., N. Taitel-Goldman, and V. Ezersky (2023), Sources and formation of iron minerals in eastern Mediterranean coastal sandy soils-A HRTEM and clay mineral study, Catena, 220, doi:10.1016/j.catena.2022.106644.

Paleomagnetism

(2022), Latest Cretaceous palaeogeographic evolution of northeast Iberia: Insights from the Campanian continental Montalban subbasin (Spain), Earth-Science Reviews, 235, doi:10.1016/j.earscirev.2022.104251.

Arkula, C., N. Lom, J. Wakabayashi, G. R. Downing, A. Qayyum, M. J. Dekkers, P. C. Lippert, and D. J. J. van Hinsbergen (2023), The forearc ophiolites of California formed during trench-parallel spreading: Kinematic reconstruction of the western USA Cordillera since the Jurassic, Earth-Science Reviews, 237, doi:10.1016/j.earscirev.2022.104275.

Di Vincenzo, G. (2022), High precision multi-collector Ar-40/Ar-39 dating of moldavites (Central European tektites) reconciles geochrological and paleomagnetic data, Chemical Geology, 608, doi:10.1016/j.chemgeo.2022.121026.

Dongre, A., P. S. Dhote, P. Zamarkar, S. J. Sangode, G. Belyanin, D. C. Meshram, S. K. Patil, A. Karmakar, and L. Jain (2022), Short-lived alkaline magmatism related to the Reunion plume in the Deccan Large Igneous Province: inferences from petrology, Ar-40/Ar-39 geochronology and palaeomagnetism of lamprophyre from the Sarnu-Dandali Alkaline Igneous Complex, in LAMPROPHYRES, LAMPROITES AND RELATED ROCKS: Tracers to Supercontinent Cycles and Metallogenesis, edited by L. Krmicek and N. V. C. Rao, pp. 381-411, doi:10.1144/sp513-2021-34.

Kovalenko, D. V. (2022), Paleomagnetism of the Silurian and Devonian Thicknesses of Southern and Central Tuva, Izvestiya-Physics of the Solid Earth, 58(6), 782-814, doi:10.1134/s1069351322060076.

Li, Z. Y., L. Ding, A. K. Laskowski, W. B. Burke, Y. F. Chen, P. P. Song, Y. H. Yue, and J. Xie (2022), New Paleomagnetic Constraints on the Early Cretaceous Paleolatitude of the Lhasa Terrane (Tibet) (vol 10, 785726, 2022), Frontiers in Earth Science, 10, doi:10.3389/feart.2022.953708.

Liang, H., et al. (2023), Stepwise northward compression in the northeastern Tibetan Plateau: Insights from the chronology of the Baima Basin, Global and Planetary Change, 220, doi:10.1016/j.gloplacha.2022.104015.

Ma, Y. M., W. M. Ruan, C. Niu, and T. S. Yang (2022), Movement History of the Microcontinents from the Tibetan Plateau Based on Paleomagnetic Results with Sufficient Sampling Units, Journal of Earth Science, 33(5), 1072-1080, doi:10.1007/s12583-022-1721-2.

Marton, E., V. Cosovic, G. Imre, and M. Velki (2022), Changing directions of the tectonic structures, consistent paleomagnetic directions at the NE imbricated margin of Stable Adria, Tectonophysics, 843, doi:10.1016/j.tec-

to.2022.229594.
Mendes, M. N., L. M. Lobato, F. Caxito, C. A. Rosiere, C. Lana, and R. Silva (2022), Episodic mafic dike swarms (2.0 and 1.7 Ga) in the Quadril acute accent atero Ferrifero Province, Brazil: Implications for the refinement of the Sa tilde o Francisco Craton magmatic barcode and the North China link, Journal of South American Earth Sciences, 120, doi:10.1016/j.jsames.2022.104049.
Metelkin, D. V., E. V. Vinogradov, V. V. Shcherbakova, V. A. Vernikovsky, S. M. Zakharov, and K. E. Nagovitsin (2022), Concerning Paleogeographic Reconstructions and the State of the Geomagnetic Field at the Precambrian-Paleozoic Boundary: New Paleomagnetic Data for the Olenek Uplift (Siberian Craton), Doklady Earth Sciences, 506(2), 710-715, doi:10.1134/s1028334x22600414.
Niu, C., et al. (2023), The Cretaceous stationary Lhasa terrane constrained by the paleolatitude of 103 Ma volcanic rocks from the Nima area, Global and Planetary Change, 220, doi:10.1016/j.gloplacha.2022.103998.
Pavlov, V. E., D. V. Rud'ko, S. A. Fursova, and T. E. Bagdasaryan (2022), Metachronous Remagnetization of the Ordovician Rocks of Moyero River Key Section (Northern Siberian Platform): Duration and Probable Mechanism, Izvestiya-Physics of the Solid Earth, 58(6), 815-841, doi:10.1134/s1069351322060106.
Perez-Valera, L. A., J. J. Villalain, F. Perez-Valera, A. Azor, and M. Sanchez-Gomez (2022), Variably rotated lamproite dikes within a transpressive fault zone: Structural and paleomagnetic analysis of the Socovos Fault zone (Eastern Betics, SE Spain), Journal of Structural Geology, 165, doi:10.1016/j.jsg.2022.104746.
Sager, W. W., and C. Carvallo (2022), Paleomagnetism and paleolatitude of igneous drill core samples from the Izu-Bonin forearc and implications for Philippine Sea plate motion, Tectonophysics, 841, doi:10.1016/j.tecto.2022.229573.
Salminen, J., S. A. Elming, and P. Layer (2023), Timing the break-up of the Baltica and Laurentia connection in Nuna-Rapid plate motion oscillation and plate tectonics in the Mesoproterozoic, Precambrian Research, 384, doi:10.1016/j.precamres.2022.106923.
Salnaia, N. V., Y. V. Rostovtseva, O. V. Pilipenko, and A. S. Kudashin (2022), Palaeomagnetism of the Sarmatian-Maeotian of the Eastern Paratethys: Remagnetization or Not?, Izvestiya-Physics of the Solid Earth, 58(6), 882-901, doi:10.1134/s1069351322060118.
Waldron, J. W. F., P. J. A. McCausland, S. M. Barr, D. I. Schofield, D. Reusch, and L. Wu (2022), Terrane history of the Iapetus Ocean as preserved in the northern Appalachians and western Caledonides, Earth-Science Reviews, 233, doi:10.1016/j.earscirev.2022.104163.
Wei, B. T., et al. (2022), Placing Another Piece of the Tethyan Puzzle: The First Paleozoic Paleomagnetic Data From the South Qiangtang Block and Its Paleogeographic Implications, Tectonics, 41(10), doi:10.1029/2022tc007355.

Software and databases

Bai, F., L. Chang, P. F. Xue, and S. S. Wang (2022), Decomposing isothermal remanent curves and development of a batch processing tool BatchUnMix, Chinese Journal of Geophysics-Chinese Edition, 65(12), 4789-4801, doi:10.6038/cjg2022Q0232.
Pisarevsky, S. A., Z. X. Li, M. G. Tetley, Y. Liu, and J. P. Beardmore (2022), An updated internet-based Global Paleomagnetic Database, Earth-Science Reviews, 235, doi:10.1016/j.earscirev.2022.104258.

Stratigraphy

Bakhmutov, V., and D. Hlavatskyi (2022), On the reliability of a stratigraphic interpretation that overlooks geophysical techniques and results when determining the age of loess-soil deposits e Comment on Lanczont et al. (2022) "A remarkable last glacial loess sedimentation at Roxolany in the Dniester Liman (Southern Ukraine)", Quaternary Science Reviews, 297, doi:10.1016/j.quascirev.2022.107668.
Lanczont, M., P. Mroczek, M. Komar, S. Fedorowicz, B. Woronko, J. Nawrocki, Z. Frankowski, and K. Standzikowski (2022), Reply to the comment on "A remarkable last glacial loess sedimentation at Roxolany in the Dniester Liman (Southern Ukraine)" Lanczont et al, Quaternary Science Reviews, 297, doi:10.1016/j.quascirev.2022.107835.
Malaguti, A. B., S. Branca, F. Speranza, M. Coltelli, P. Del Carlo, and A. Renzulli (2023), Age of the Valle del Bove formation and chronology of the post-collapse flank eruptions, Etna volcano (Italy), Journal of Volcanology and Geothermal Research, 434, doi:10.1016/j.jvolgeores.2023.107752.

Volcanology

Okumura, S., K. Uesugi, A. Goto, T. Sakamaki, K. Matsumoto, A. Takeuchi, and A. Miyake (2022), Rheology of nanocrystal-bearing andesite magma and its roles in explosive volcanism, Communications Earth & Environment, 3(1), doi:10.1038/s43247-022-00573-9.

cont'd. from pg. 1...

complex quantity, with $\chi = \chi' - i\omega\chi''$, where χ' is the in-phase response and χ'' is the out-of-phase susceptibility. Paramagnetic and diamagnetic materials have responses that are perfectly in-phase with the oscillating field; therefore these materials have no frequency dependent behavior and $\chi'' = 0$.

The delayed response and corresponding out-of-phase susceptibility can arise from three distinct physical mechanisms: (1), magnetic viscosity with relaxation times comparable to the AC field reversal interval; (2), irreversible magnetization changes (low-field hysteresis) driven by the AC field; and (3), production of electrical eddy currents by the AC field in electrically conductive materials (see Jackson (2003), IRMQ 13-4) for more detail). Each of these mechanisms is significant only for a restricted range of materials: viscosity on millisecond timescales (for frequencies typically available in susceptometers at the IRM) is generally only important for fine SD particles, near the SP boundary. Low-field hysteresis has been documented only in multidomain pyrrhotite, hematite, and intermediate composition titanomagnetites, where spontaneous magnetization is not too large and wall-pinning energies are comparable to external-field interaction (Zeeman) energies. Conductivity is only large enough to matter in metals, graphite and some sulfide minerals, in the frequency range commonly used for susceptibility measurements. Quadrature susceptibility χ'' is therefore almost always much smaller than in-phase susceptibility χ'. But when it is significant in magnitude, it provides important information about the magnetic (and/or conductive) mineral assemblage.

For very small SD ("viscous superparamagnetic" or VSP) grains, χ'' and the frequency dependence of χ' (frequency $f = \omega/2\pi$) are closely related to viscous changes of M_r with time t (Néel, 1949; Mullins & Tite, 1973; Shcherbakov & Fabian, 2005; Egli, 2009). For low frequencies and/or short relaxation times ($\omega\tau << 1$), the assemblage is superparamagnetic and M stays in phase and in equilibrium with the changing field: $M(t) = \chi_{SP}H(t) = M_{eq}(H_0)H(t)/(H_0)$. With increasing frequency and/or relaxation time τ, the time constants for measurement and relaxation become comparable ($\tau/\tau_m \sim \omega\tau \sim 1$), and the magnetization becomes more "viscous," lagging significantly, with roughly equal in-phase and quadrature components: $M' \sim M'' \sim M\mathrm{eq}(H_0)/2$. Finally, for very high ω and/or very long τ, the grains reach the stable SD state ($\chi'' \rightarrow 0$). Néel (1949) showed that for grains with a wide distribution of relaxation times, the quadrature signal is proportional to the frequency-dependence of the in-phase susceptibility, through the useful "$\pi/2$" law: $\chi''[\text{viscosity}] = -(\pi/2)(\delta\chi'/\delta \ln f)$. The $\pi/2$ law was adapted by Mullins and Tite (1973) for thermal activation energies.

However, the observations above have also been made for (much) larger MD grains at temperatures < 70 K, see Fig. 1, so that their origin must be distinguished and understood, making for the focus of this article. Before discussing the behavior of MD magnetite grains in detail, and to summarize the occurrences of frequency and amplitude field dependencies of both χ' and χ'' for different minerals/domain states, the table from the IRMQ28-2 is presented again here yet correcting the erroneous inclusion of amplitude-dependence of SP grains of the previous version. It is also important to clarify that all observations for magnetite-titanomagnetite are from grains larger than 2-3 μm, therefore all MD grains, whereas SD grains, with long relaxation times and no low-field hysteresis are void of frequency- and amplitude- dependencies.

Mineral/domain state	**Frequency (Hz)-dependency**	**Field (H_{AC})-dependency**	**References**
SP grains	χ', χ''		Mullins and Tite (1973)
Pyrrhotite	χ', χ''	χ', χ'' Eddy currents	Worm (1991); Worm et al. (1993); Volk et al. (2018)
SD	*	*	Worm (1998)
MD mgt	$\lesssim$ 50 K: χ', χ'', $\pi/2$ peak Relaxation of domain walls	< 120 K: χ', χ'' Domain-wall pinning low-field hysteresis **	Moskowitz et al. (1998); Özdemir et al. (2009); Jackson et al. (1998)
MD ti-mgt	@ 250 K: χ', χ'' Reorientation of interstitial Fe^{2+} defects, composition-dependent $\lesssim$ 70 K: χ', χ'', $\pi/2$ peak Relaxation of domain walls	$\gtrsim$ 150 K: χ', χ'' Low-field hysteresis, (T varies with composition)	Jackson et al. (1998); Moskowitz et al. (1998); Carter-Stiglitz et al. (2006); Church et al. (2011)
MD hmt	$\gtrsim$ 260K: χ', χ'', $\pi/2$ peak		Rock Magnetic Bestiary
Ti-hmt		$\lesssim$ 210 K: χ', χ'' Low-field hysteresis (T varies with composition)	Lagroix et al. (2004)

Summary of known magnetic susceptibility observations for different minerals and grain sizes: χ' is in-phase susceptibility; χ'' is out of phase susceptibility; $\pi/2$ indicates the viscosity parameter of Mullins and Tite (1973). *: stable SD grains have long relaxation times, so that frequency-dependence is not observed. Likewise, SD grains do not possess low-field hysteresis residing in irreversible domain wall modification, so that amplitude-dependence is also not present. **: minor, almost negligible, amplitude-dependence of χ' was described by Jackson et al. (1998) for magnetite when measuring in fields greater than ~100 A/m, and more significant χ'' by Özdemir et al. (2009).

Multidomain Magnetite

For a synthetic 1-2 mm spherical magnetite crystal, Moskowitz et al. (1998) observed step-like increases in χ' during heating at 40-50 K and 120-125 K. The higher temperature increase is coincidental with the Verwey transition (T_V) and accompanied by changes in the SIRM heating curve, however, the lower-temperature step has no matching remanence transition, it is frequency-dependent, and is accompanied by a peak in χ''. Similar χ(T) variations were observed by Muxworthy (1999) for disperse hydrothermal magnetite crystals with mean sizes of 76 and 108 μm, with somewhat smoother increases in χ', and slight frequency-dependence between 118-126 K, in 1 K intervals, over the 40- 4,000 Hz frequency range. In a study by Kosterov (2003), only 100-150 μm

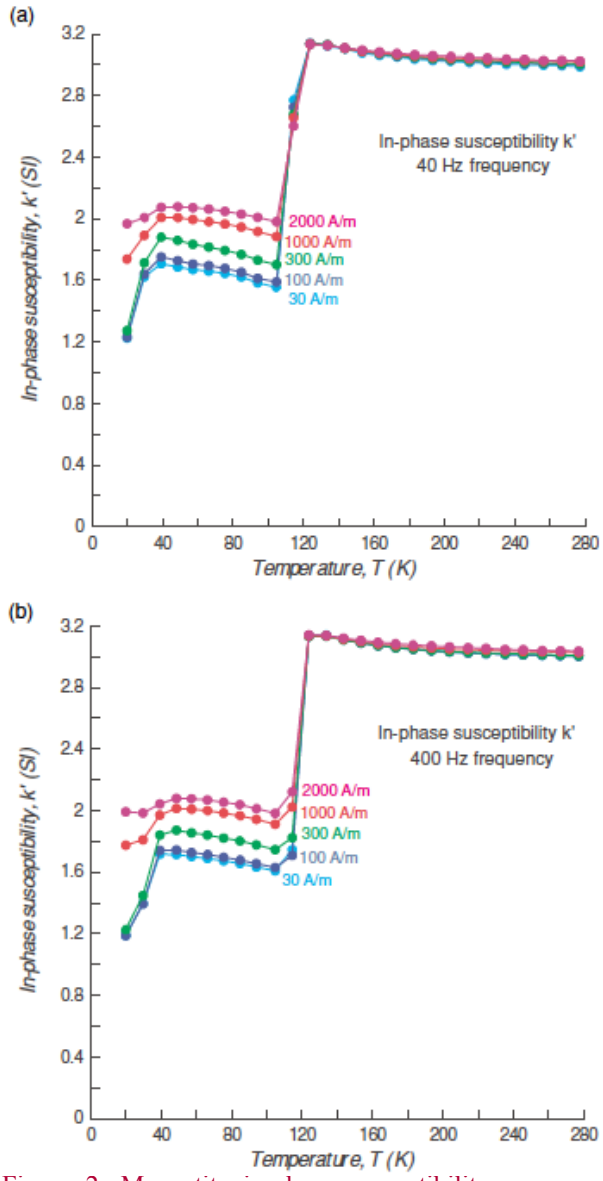

Figure 2: Magnetite in-phase susceptibility measurements as a function of amplitude and temperature for two measurement frequencies of (a) 40 Hz and (b) 400 Hz. Note the pronounced amplitude-dependence < 120 K and negligible, yet present, above (from Özdemir et al., 2009).

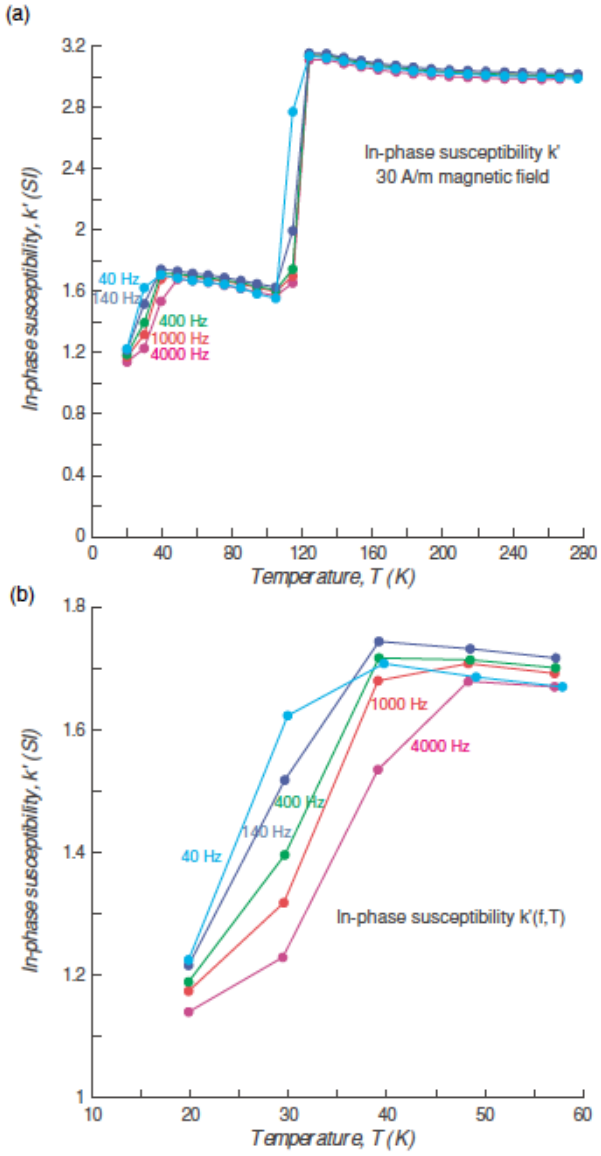

Figure 3: Magnetite in-phase susceptibility measurements as a function of frequency and temperature for amplitudes between 40-4,000 Hz, between 20 and 280 K (a). (b) enlargement of the 20-60 K range. (From Özdemir et al., 2009).

crushed size fractions of natural magnetite showed clear double-step increases of χ' at low T, one at 120-125 K, associated with a Hopkinson peak around 135 K, and one from 15-30 K, then gently descending between 30 and 120 K. Frequency-dependence of χ' on the order of 10-15% was also observed between 0.01 and 1,000 Hz in the same study. For a synthetic magnetite cylinder with 4 mm diameter and 13 mm height measured in an AC field of 80 A/m and single frequency of 100 Hz, Skumryev et al. (1999) also observed an increase in χ' around 50 K followed by a steady drop until ~120 K, at which point χ' increased markedly and was followed by a Hopkinson peak around 130 K. Additionally, they reported a χ" peak just below 50 K. A marked frequency-dependence of both χ' and χ" behaviors was demonstrated when measuring in 10, 30, 100, 300 and 1,000 Hz between 10 and 80 K, with the most prominent dependence between 20 and 70 K.

Finally, Özdemir et al (2009) performed the most detailed study to date, investigating both frequency- (40-4,000 Hz) and amplitude- (30-2,000 A/m) dependence of a natural 1.7 mm octahedral magnetite single-crystal. In their study, marked amplitude dependence of in-phase susceptibility was observed below the Verwey transition for two measurement frequencies (Fig. 2), accompanied by frequency dependence, particularly <50 K, although some was also observed in the 95-125 K range. Above the T_V the field dependence of χ' was described as "very nearly zero", and then discussed as non-existent by virtue of χ reaching the $1/N$ limit, where N is the demagnetizing factor.

Out-of-phase susceptibility, instead, was observed to possess a frequency-dependent peak ~30 K, and some frequency dependence above that, particularly for the

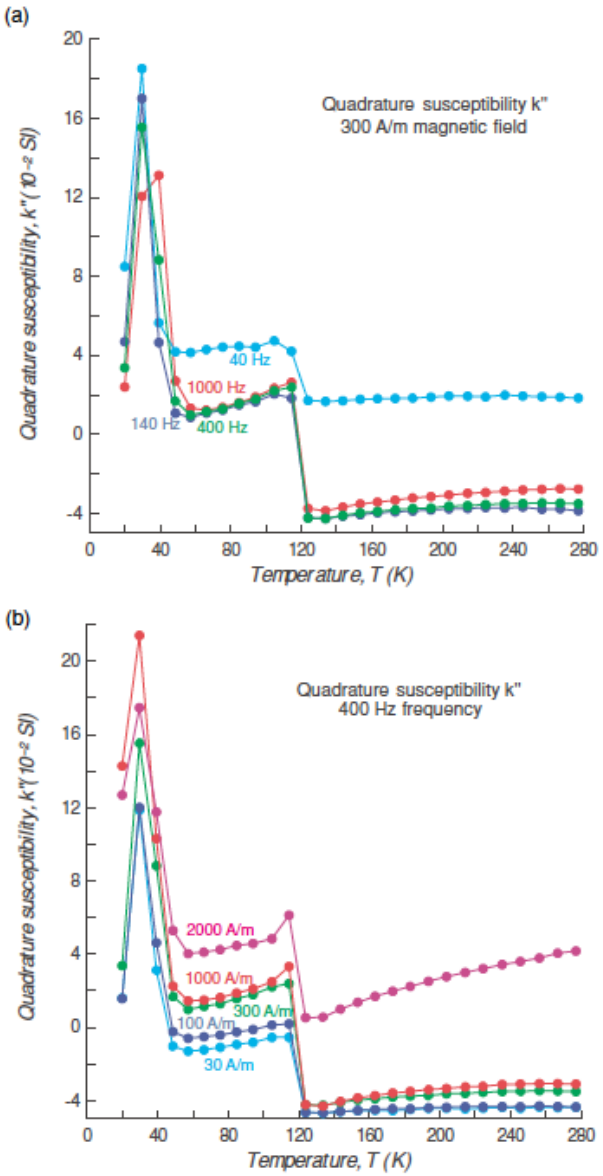

Figure 4: Magnetite out-of-phase susceptibility measurements (a) as a function of frequency and temperature for an amplitude of 300 A/m, and (b) as a function of amplitude and temperature for a frequency of 400 Hz. Note, the negative χ" values, particularly > 120 K, which were attributed to instrumental artifacts (From Özdemir et al., 2009).

lowest measurement frequency (40 Hz), and a marked drop/increase at the T_V, although negative measurements were attributed to instrumental artifacts (Fig. 4a). χ" also revealed amplitude dependence above and below T_V (Fig. 4b). Even discounting measurements in the strongest field of 2,000 A/m (2.5 mT), at least at the scale of the figure the dependence is apparent for all fields < T_V and for fields greater than 100 A/m (125 μT) > T_V.

Assuming that the sample possesses a minimal field dependence of χ', the results would be consistent with the room temperature observation of χ' for TM0 (magnetite) in fields > 100 A/m of Jackson et al. (1998), also reported in the IRMQ28-2, although at typical measurement amplitudes (MD) magnetite is effectively field- and frequency-independent above T_V.

The 20-40 K frequency and amplitude dependent step in χ' and peak in χ" are similar to those reported by other authors, yet there is some disagreement about the temperature range over which they occur, which appears to be irrespective of measurement frequency. For example, Iwauchi et al. (1976) observed similar temperature ranges as Özdemir et al. (2009), yet the frequencies used there were three orders of magnitude higher. Likewise, Janů et al. (2007) reported the same temperature range, yet using much lower frequencies (1-25 Hz). For similar frequencies (10-1000 Hz), the "step and peak" features of χ' and χ", respectively, observed by Skumryev et al. (1999) are broader, occurring between 30-50 K. Only exception to these, are the observations of Balanda et al. (2005) who, for a stoichiometric synthetic magnetite crystal, reported frequency independent step decreases in χ' and minor peaks in χ" at 28 K, not seen in the other studies. They do observe frequency-dependent step increases in χ' and major peaks in χ", for a frequency range of 15-1,000 Hz, similar to that of Özdemir et al. (2009), but between 50 and 60 K. Furthermore, only for their lowest 80 A/m field were these steps and peaks clear, but were otherwise subdued and unresolvable at higher fields. Considering the similarities in instrumentation used, Özdemir et al. (2009) attributed the different observations to subtle differences in composition and purity, and on the method of preparation of the synthetic material.

For a thermally activated process, the relaxation time, $\tau = (2\pi f)^{-1}$, obeys the Arrhenius equation:

$$\tau = \tau_0 \exp [E_a/(k_B T)]$$

where f is the measurement frequency, τ_0 is the characteristic attempt time, Ea is the activation energy and k_B is the Boltzmann constant. Hence a plot of ln(τ) versus 1/T yields a straight line with slope E_a/k_B and intercept ln(τ_0)

Activation Energies E_a and characteristic non-thermal response time τ_0 estimates calculated by Özdemir et al. (2009) and Carter-Stiglitz et al. (2006) from the frequency-dependence of χ', and Skumryev et al. (1999) from the frequency dependence of the χ" peak are in agreement, and match closely with the activation energies of conduction by electron hopping for the same temperatures (Lenge & Kronmuller, 1984). These observations support the idea that electron mobility/valence changes within domain walls are at the root of the frequency-dependent variations in susceptibility around 30-40 K (Walz et al., 1982; Moskowitz et al., 1998; Muxworthy, 1999).

The mechanism, however, is not as clear. While the sharp step in SIRM (not shown here) and susceptibility curves at T_V observed by Özdemir et al. (2009) represent a large change in anisotropy, the lack of any feature in SIRM below 40 K, if attributed to domain wall pinning, would require major lattice defects, however this is not necessarily the case for susceptibility. Özdemir et al. (2009) suggested that while the walls do remain pinned, perhaps near monoclinic twin boundaries, wall segments oscillate reversibly in the alternating fields, with the amplitude of oscillation changing steadily in the

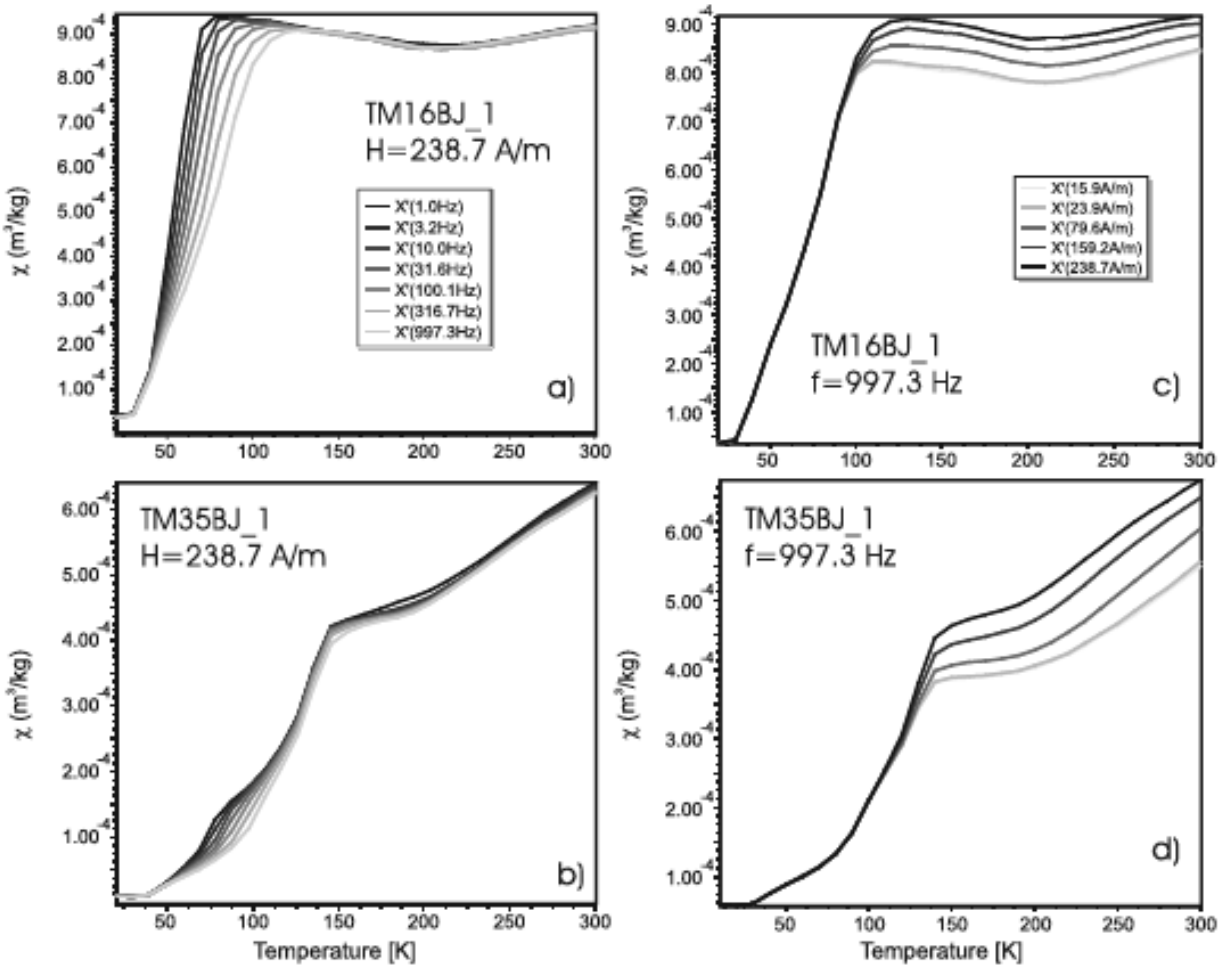

Figure 5: A and B: in-phase susceptibility as a function of frequency and temperature (fixed amplitude) for titanomagnetite compositions x= 0.16 and 0.35, respectively; C and D: in-phase susceptibility as a function of amplitude and temperature (fixed frequency) for the same samples. Results beautifully demonstrate the frequency dependence below a certain temperature, 100 and 150 K, respectively, for these two samples, and amplitude dependence above. From Carter-Stiglitz et al. (2006).

20-40 K range. Here, χ" peaks and the temperature at which χ' increases on warming changes with frequency, generating the "step and peak" feature. Wall oscillations lag appreciably behind the driving field at these very low temperatures, becoming more prominent with increasing frequency.

Multidomain Titanomagnetite

Carter-Stiglitz et al. (2006) studied two synthetic samples of composition x= 0.16 and x= 0.35 to investigate field cooled and zero-field cooled behavior. They observed strong frequency-dependence at low temperatures, < 100 and 150 K, respectively, and amplitude-dependence above (Fig. 5). The temperature at which the different behaviors occur was proposed to be associated with changes in grain anisotropy associated with electron hopping in the octahedral sites and is therefore dependent on composition.

Church et al. (2011) investigated the low temperature susceptibility behavior in a series of synthetic MD titanomagnetites of composition 0< x< 0.6, in conjunction with low-temperature FORC and remanence measurements. For the x= 0.2, 0.4 compositions they report on, they observed similar low temperature susceptibility features to those described here yet centered around ~70 K and with an additional low-temperature shoulder on the χ" peak (Fig. 6). As advanced by Özdemir et al. (2009), these results support the suggestion that the temperature at which the susceptibility features occur are compositionally dependent.

Additionally, Church et al. (2011) described two domain wall relaxation regimes acting on titanomagnetites of varying compositions. For compositions greater than x= 0.2, Fe^{2+} ions enter the tetrahedral sites (O'Reilly & Banerjee, 1965), introducing magnetoelastic contributions to the anisotropy, which generate wall pinning. However, these alone are insufficient to cause the effect observed, so that enhanced pinning is further promoted by localization of Fe^{2+} ions on the octahedral sublattice due to cessation of electron hopping (magnetocrystalline anisotropy). Church et al. (2011) suggest that a similar mechanism operates at x> 0.2 and that enhanced pinning for these compositions, below the low-temperature relaxation, i.e. ~70 K, is predominantly magnetoelastic in origin. This way, Church et al. (2011) distinguish between an intrinsic pinning low-temperature regime from an extrinsic regime dominated by defects such as dislocations, grain boundaries, impurities, etc. The two re-

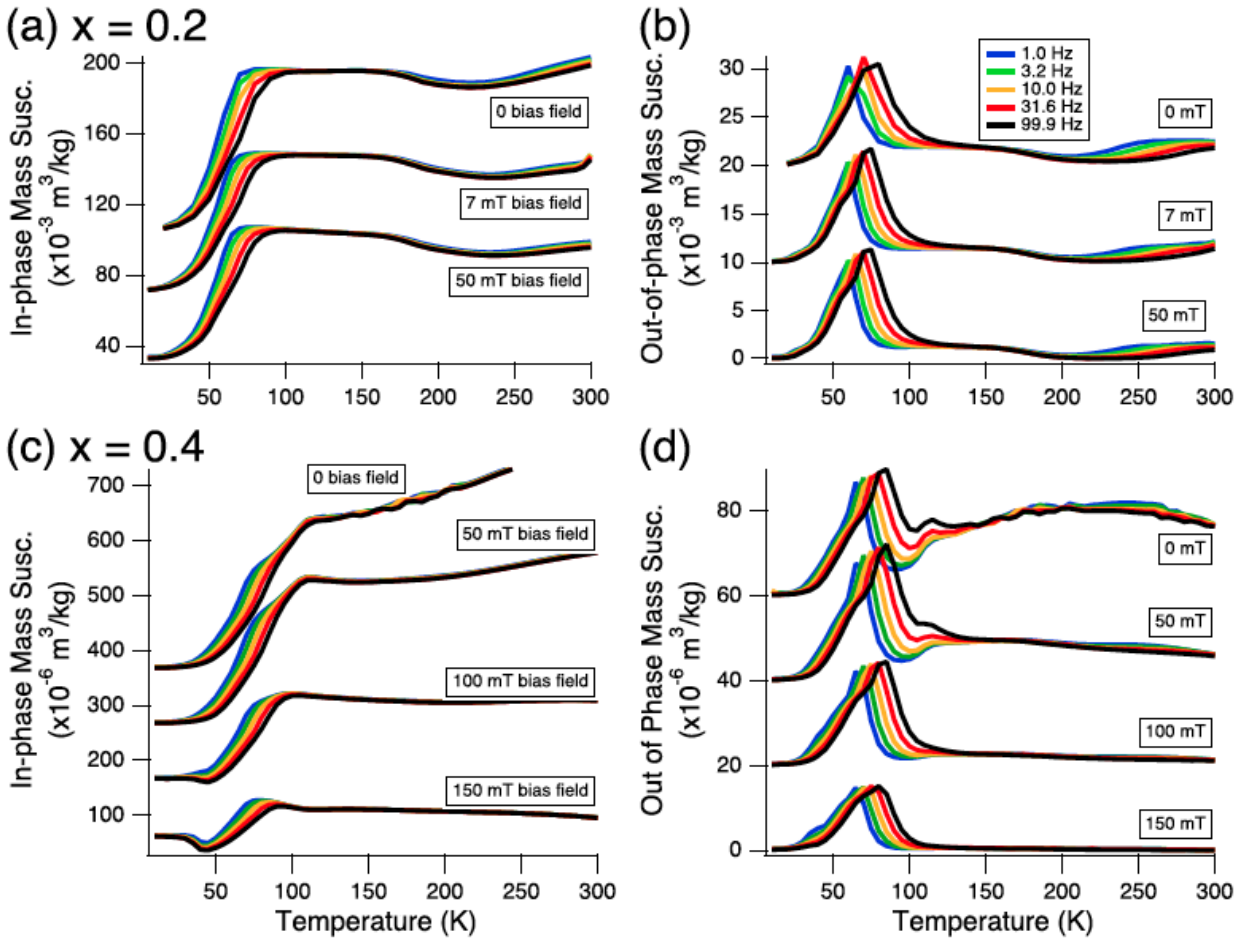

Figure 6: Frequency dependence of magnetic susceptibility for compositions (a and b) x = 0.2 and (c and d) x = 0.4 at low temperatures and with bias fields from 0 to 150 mT. Graphs are offset on the y axis, but the scale is preserved (From Church et al., 2011).

gimes may be discriminated by large difference in ZFC and FC remanence curves below the pinning transition, which would not be otherwise observed if pinning were entirely caused by extrinsic defects. The intrinsic pinning regime also predicts that domain walls are rigidly pinned along their entire length, whereas in the extrinsic pinning regime walls are only pinned at discrete points, permitting sections of wall in between pinning sites to bow in response to an applied field, as proposed by Özdemir et al. (2009) for stoichiometric magnetite compositions.

Summary and Final Remarks

In summary, a step in χ' between ~20-70 K accompanied by a same-temperature peak in χ" is indicative of electron hopping associated with domain wall relaxation in MD magnetite-titanomagnetite. The temperature at which these features occur is dependent on composition and stoichiometry, with somewhat higher temperatures (~50-70 K) for titanomagnetite compared to stoichiometric magnetite (~20-50 K). For all compositions, the low temperature relaxation feature is both frequency- and amplitude- dependent; however, only titanomagnetite will possess appreciable amplitude-dependence and no frequency-dependence between ~150 K and room temperature.

For stoichiometric magnetite, the low-temperature (< T_V) "MD feature" may be distinguished from SP grains by its amplitude dependence, which is absent when titanium is present, and resides in low-field hysteresis. For all compositions, the temperature range over which the frequency-dependent features occur, while broad-ish (20-70 K), is more "fixed" than the SP blocking peak, which varies widely with mean blocking volume, and extends from as low to a few K for the smallest SP grains ("unstable SD"), to above room temperature for stable SD grains (e.g., Till et al., 2011).

For all compositions, the frequency-dependent relaxation resulting in the χ' step and χ" peak is a thermally activated relaxation process, as confirmed by it following an Arrhenius equation. Such behavior thus also follows the $\pi/2$ law for distribution of relaxation times (Néel, 1949) readapted for thermal activation energies (Mullins and Tite, 1973), so that the χ" frequency-dependent peak can be successfully reproduced from the χ'-frequency data as χ"[viscosity]= $-(\pi/2)(\delta\chi'/\delta \ln f)$.

For certain titanomagnetite compositions, e.g., x= 0.2 but not x= 0.4, a second relaxation for in χ" is observed around 250 K (Church et al., 2011, Fig. 6), which had been attributed to diffusional reorientation of interstitial Fe^{2+} defects (Walz et al., 1997). However, the feature in χ" is never a peak, but more of a broad frequency-dependent step (x= 0.2) or "hump" (x= 0.4), accompanied by an increased gradient in χ' towards room temperature

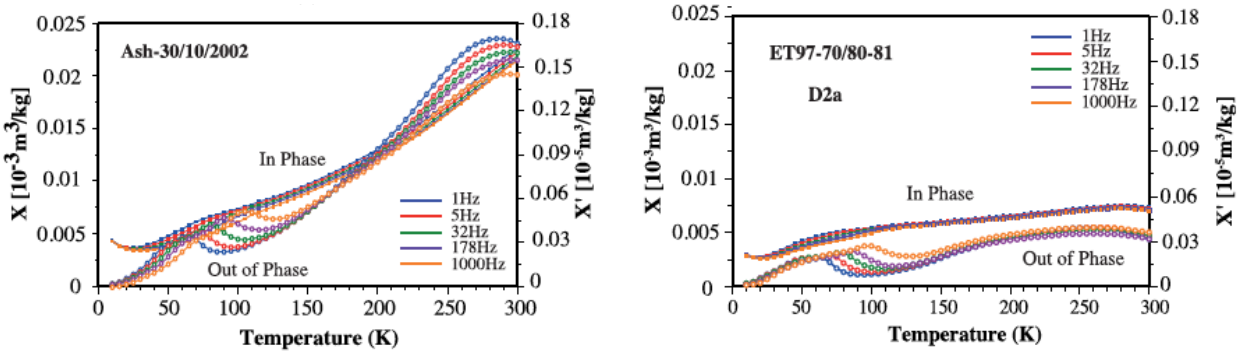

Figure 7: Natural titanomagnetite-bearing volcanic ash samples from Vigliotti et al. (2022). Left, highly fractionated samples of estimated composition x= ~0.6, with steep χ (in-phase susceptibility in their figure) gradient towards room temperature and a prominent frequency-dependent χ' (here used to indicate out-of-phase susceptibility) peak attributed to the superposition of a SP-SD distribution and the specific titanomagnetite features described in this article; Right, less fractionated sample of estimated composition x= ~0.2. Both samples display prominent low temperature frequency-dependent "step and peak" features in in-phase and out-of-phase susceptibility, respectively.

(Figs. 5 and 6). The gradient in χ' increases for increasing titanium substitution (Moskowitz et al., 1998) and reasonably extends above room temperature up to the specific Curie temperature.

It is problematic, however, to attribute the characters of these curves exclusively to titanium content in natural samples where mineralogical and/or grain size mixtures may exist. For example, Vigliotti et al. (2022) reported on different compositions of titanomagnetite-bearing volcanic ashes with contrasting coercivity distributions, as determined by hysteresis shape, IRM unmixing, FORC distributions and remanence curves, in addition to SEM observations. Indeed, the higher Ti-containing samples (e.g., Ash-30/10/2002 in Fig. 7) possessed an increased gradient of χ' towards room temperature as described above, but the same highly fractionated samples also feature broad and prominent frequency-dependent peaks in χ" (the classic "rainbows") between ~150 K and room temperature (Fig. 7, left). Such broad frequency-dependence, should not occur for MD (titano)magnetites, which only display amplitude dependence in this temperature range, other than the 250 K feature observed for certain titanomagnetite compositions (Cf. Fig. 6b). The increase of χ', instead, likely peaks above room temperature towards the Curie temperature. In virtue of these, as well as other rock-magnetic observations, these features were attributed to a prominent distribution of SP grains, some blocking above room temperature, and resulting in the heightened coercivity contrast in those samples, in addition to the lower-temperature MD features that are the main focus of this review.

References

Carter-Stiglitz, B., Moskowitz, B., Solheid, P., Berquó, T. S., Jackson, M., & Kosterov, A. (2006). Low-temperature magnetic behavior of multidomain titanomagnetites: TM0, TM16, and TM35. Journal of Geophysical Research: Solid Earth, 111(B12), n/a-n/a. https://doi.org/10.1029/2006JB004561

Church, N., Feinberg, J. M., & Harrison, R. (2011). Low-temperature domain wall pinning in titanomagnetite: Quantitative modeling of multidomain first-order reversal curve diagrams and AC susceptibility. Geochemistry, Geophysics, Geosystems, 12(7), n/a-n/a. https://doi.org/10.1029/2011GC003538

Egli, R. (2009). Magnetic susceptibility measurements as a function of temeperature and freqeuncy I: inversion theory. Geophysical Journal International, 177(2), 395–420. https://doi.org/10.1111/j.1365-246X.2009.04081.x

Iida, S., Mizushima, K., Yamada, N., & Iizuka, T. (1968). Details of the Electronic Relaxation in MnxFe3−xO4+γ. Journal of Applied Physics, 39(2), 818–819. https://doi.org/10.1063/1.2163625

Iwauchi, K., Koizumi, N., Kiyama, M., & Bando, Y. (1976). Magnetic Relaxation in FeO and Ferrites. Bulletin of the Institute for Chemical Research, Kyoto University, 54(4), 255–262.

Jackson, M. J. (2003). Imaginary Susceptibility - A Primer. IRM Quarterly, 13(4), 1–12.

Jackson, M. J., Moskowitz, B., Rosenbaum, J., & Kissel, C. (1998). Field-dependence of AC susceptibility in titanomagnetites. Earth and Planetary Science Letters, 157(3–4), 129–139. https://doi.org/10.1016/S0012-821X(98)00032-6

Janů, Z., Hadač, J., & Švindrych, Z. (2007). Glass-like and Verwey transitions in magnetite in details. Journal of Magnetism and Magnetic Materials, 310(2), e203–e205. https://doi.org/10.1016/j.jmmm.2006.10.344

Kosterov, A. (2003). Low-temperature magnetization and AC susceptibility of magnetite : effect of thermomagnetic history. Geophysical Journal International, 154, 58–71.

Lagroix, F., Banerjee, S. K., & Jackson, M. J. (2004). Magnetic properties of the Old Crow tephra: Identification of a complex iron titanium oxide mineralogy. Journal of Geophysical Research: Solid Earth, 109(B1). https://doi.org/10.1029/2003JB002678

Lenge, N., & Kronmuller, H. (1984). Electrical conductivity and magnetic aftereffect in the ordered phase of magnetite. Adv. Ceramics, 15, 331–339.

Moskowitz, B. M., Jackson, M. J., & Kissel, C. (1998). Low-temperature magnetic behavior of titanomagnetites. Earth and Planetary Science Letters, 157(3–4), 141–149. https://doi.org/10.1016/S0012-821X(98)00033-8

Mullins, C. E., & Tite, M. S. (1973). Magnetic viscosity, quadrature susceptibility, and frequency dependence of susceptibility in single-domain assemblies of magnetite and maghemite. Journal of Geophysical Research, 78(5), 804–809. https://doi.org/10.1029/JB078i005p00804

Muxworthy, A. R. (1999). Low-temperature susceptibility and hysteresis of magnetite. Earth and Planetary Science Letters, 169(1–2), 51–58. https://doi.org/10.1016/S0012-821X(99)00067-9

Néel, L. (1949). Théorie du traînage magnétique des ferromagnétiques en grains fins avec applications aux terres cuites. Annales de Geophysique, 5(99–136).

O'Reilly, W., & Banerjee, S. K. (1965). Cation distribution in titanomagnetites (1 − x)Fe3O4 − xFe2TiO4. Physics Letters, 17(3), 237–238. https://doi.org/https://doi.org/10.1016/0031-9163(65)90504-4

Özdemir, Ö., Dunlop, D. J., & Jackson, M. (2009). Frequency and field dependent susceptibility of magnetite at low temperature. Earth, Planets and Space, 61(1), 125–131. https://doi.org/10.1186/BF03352892

Shcherbakov, V. P., & Fabian, K. (2005). On the determination of magnetic grain-size distributions of superparamagnetic particle ensembles using the frequency dependence of susceptibility at different temperatures. Geophysical Journal International, 162(3), 736–746. https://doi.org/10.1111/j.1365-246X.2005.02603.x

Skumryev, V., Blythe, H. J., Cullen, J., & Coey, J. M. D. (1999). AC susceptibility of a magnetite crystal. Journal of Magnetism and Magnetic Materials, 196, 515–517. https://doi.org/10.1016/S0304-8853(98)00863-4

Till, J. L., Jackson, M. J., Rosenbaum, J. G., & Solheid, P. (2011). Magnetic properties in an ash flow tuff with continuous grain size variation: A natural reference for magnetic particle granulometry. Geochemistry, Geophysics, Geosystems, 12(7), n/a-n/a. https://doi.org/10.1029/2011GC003648

Vigliotti, L., Bilardello, D., Winkler, A., & Del Carlo, P. (2022). Rock magnetic fingerprint of Mt Etna volcanic ash. Geophysical Journal International, 231(2), 749–769. https://doi.org/10.1093/gji/ggac213

Volk, M. W. R., Jackson, M. J., & Bilardello, D. (2018). Magnetic tests and characterization protocols: mineralogy and grain size / domain state Part I: isothermal strong field tests. The IRM Quarterly, 27(4), 1–21.

Walz, F., Brabers, V. A. M., Chikazumi, S., Kronmuller, H., & Rigo, M. O. (1982). Magnetic After-Effects in Single- and Poly-Crystalline Magnetite. Phys. Stat. Sol, b(110), 471–478.

Walz, F., Torres, L., Bendimya, K., de Francisco, C., & Kronmuller, H. (1997). Analysis of Magnetic After-Effect Spectra in Titanium-Doped Magnetite. Phys. Stat. Sol, 164, 805–820.

Worm, H. (1991). Multidomain susceptibility and anomalously strong low field dependence of induced magnetization in pyrrhotite. Physics of the Earth and Planetary Interiors, 69, 112–118.

Worm, H. (1998). On the superparamagnetic — stable single domain transition for magnetite , and frequency dependence of susceptibility. Geophysical Journal International, 133, 201–206.

Worm, H., Clark, D., & Dekkers, M. J. (1993). Magnetic susceptibility of pyrrhotite : grain size , field and frequency dependence. Geophysical Journal International, 114, 127–137.

The IRM
Quarterly

The *Institute for Rock Magnetism* is dedicated to providing state-of-the-art facilities and technical expertise free of charge to any interested researcher who applies and is accepted as a Visiting Fellow. Short proposals are accepted semi-annually in spring and fall for work to be done in a 10-day period during the following half year. Shorter, less formal visits are arranged on an individual basis through the Facilities Manager.

The *IRM* staff consists of **Subir Banerjee**, Professor Emeritus/Founding Director; **Bruce Moskowitz**, Professor/Director; **Joshua Feinberg**, Professor/Associate Director; **Maxwell Brown, Peat Sølheid** and **Dario Bilardello**, Staff Scientists.

Funding for the *IRM* is provided by the **National Science Foundation**, the **W. M. Keck Foundation**, and the **University of Minnesota**.

UNIVERSITY OF MINNESOTA

The *IRM Quarterly* is published four times a year by the staff of the *IRM*. If you or someone you know would like to be on our mailing list, if you have something you would like to contribute (*e.g.*, titles plus abstracts of papers in press), or if you have any suggestions to improve the newsletter, please notify the editor:

Dario Bilardello
Institute for Rock Magnetism
University of Minnesota
150 John T Tate Hall
116 Church Street SE
Minneapolis, MN 55455-0128
phone: (612) 624-5049
e-mail: dario@umn.edu
www.irm.umn.edu

IRM